

Gradient Exchange Mass Spectrometry (GEMS) for Quantifying a Suite of Dissolved Gas Fluxes

Matthew Long

Adam Subhas

Scott Wankel

Abstract We developed and deployed a membrane inlet quadrupole mass spectrometer (MIMS) system for continuous monitoring within a ~*Zostera marina*~ (eelgrass) meadow in Woods Hole, Massachusetts, USA. The benthic system measured dissolved O₂, CO₂, N₂, Ar, CH₄, and H₂S at two heights spaced ~1 m apart above the seagrass canopy, enabling vertical flux calculations using the gradient exchange method when combined with velocity measurements from an acoustic Doppler velocimeter (ADV). Data was remotely telemetered using GSM cellular communication to a web-based data store with real-time monitoring dashboard. Clear concentration gradients were observed for oxygen and carbon dioxide, showing diel cycles driven by insolation and tidal forcing. Gas species were normalized to argon to control for physical gas fluxes. Methane, nitrogen, and hydrogen sulfide measurements showed variability close to the detection limit of the instrument. The MIMS system demonstrated stable performance during deployments ranging from weeks to months, though operational challenges included biofouling management, calibration, and maintenance in the marine environment. This study demonstrates the potential of MIMS and the gradient flux method for continuous biogeochemical monitoring in coastal marine ecosystems, providing high-resolution temporal data on multiple dissolved gas species simultaneously. The gradient flux approach offers advantages over traditional benthic chamber methods by maintaining natural flow conditions while enabling ecosystem-scale process measurements.

Project History

During the first year of this project, we conducted several laboratory and field tests as outlined in our proposal. Significant developments included the testing of response time and power-saving strategies, development of the GEMS underwater mass spectrometer and pumping systems and an initial short field deployment, resulting in initial gradient estimates (Figure 1).

Developments in 2022 included a long-term deployment of the GEMS system including a solar and wind-powered surface platform (Figure 2) and involvement of 2 undergraduate and an MIT-WHOI Joint Program student graduate student, a new gas equilibrator for lab-based GEMS gas-specific calibrations and a newly designed circuit board for real-time operation and communication. A longer deployment was conducted in August-September of 2022. The system operated continu-

ously for over 3 weeks before a valve failure resulted in the loss of gradient data. Issues with QMS signal to noise ratio (Figure 11), and with the gradient valve were resolved during the subsequent development period.

During the third year of this project, we continued development and conducted laboratory tests to resolve issues and improve the GEMS system. Unanticipated departures from PI Long's lab in 2023 included an engineer, a WHOI JP student, a research assistant, and a postdoc that led to substantial delays and loss of knowledge for this project. Work on signal to noise ratios in the mass spectrometer output led to a complete redesign of the GEMS lander electronics and extensive revision of the control software. We also redesigned and tested a new valve configuration to address issues during the 2022 deployment.

In 2024, new personnel (a technician, now WHOI/MIT JP PhD student, and a research associate) were trained and continued development of the GEMS system. A no-cost extension was used to move the long-term field deployment to the summer of 2025. Continued development led to completion of the project objective to use GEMS to investigate nitrogen cycling in eelgrass systems. This also allowed us to test and refine hardware and firmware developed after the 2022 field season. We built a small chamber that could be installed in eelgrass mesocosms (Figure 3) to monitor the evolution of a pulse-label of ^{15}N labeled nitrate to labeled nitrogen gas (Figure 4). recirculated water past the GEMS inlet membrane for continuous measurement of masses 28, 29, 30, and 40 (unlabeled, singly, and doubly labeled N₂, and Argon, respectively). We used this system for a series of replicate experiments among eelgrass mesocosm treatments, allowing us to compare denitrification rates (Figure 5). This development may lead to direct, automated measurements of denitrification in the field during future GEMS deployments.

The final deployment in the summer of 2025 was 4 months in duration. This deployment tested a new lander platform (Figure 6), improved control and data acquisition systems, a new pump and gradient valve system, a new telemetry data system and accompanying web dashboard (Figure 7), and a new data reduction pipeline to handle more data from longer deployments reproducibly. The methods and results below cover the system as used in 2025.

GEMS Methods

System Overview

The gradient exchange mass spectrometry (GEMS) system combines a quadrupole mass spectrometer (QMS) sampling seawater from vertically spaced high and low inlets with an acoustic doppler velocimeter (ADV) to measure the current velocity between the inlets. The measurement system is deployed as a benthic lander. A surface barge provides power and data connections via a tether. Telemetry is provided via a GSM cellular data connection. Data acquisition, system control, and telemetry are handled by microcontrollers in the lander and barge and data is duplicated at both locations. The barge uses a wind turbine and solar panels for power generation.

The 1.8 m x 1.8 m surface support platform (Figure 2) is constructed using commercial dock flotation supporting a welded aluminum frame with solar panel and wind turbine supports. A centrally positioned watertight box holds the 200AH battery, charge controller (Victron BlueSolar

MPPT 150/35), and electronics for control and communication. The barge is moored using two anchors set in opposition to maintain position and orientation. Power is provided by two 200 W South-oriented solar panels and a wind generator (Air-X Air30) producing 100 W at 8 m s⁻¹ wind velocity, feeding power through a charge controller to a 24 V, 200 Ah LiFePO₄ battery. The power system provided ample power for the lander and surface systems for the duration of the deployment. Control, data, and communication is handled by a microcontroller with custom firmware (Teensy 4.1) in the surface electronics box. Commands and data between barge and lander use the UDP protocol over 100baseT wired ethernet, and time correction, GPS position, and GSM telemetry are provided via a serial connection to a GSM/GPS module.

Data is transmitted and received via a GSM network connection. The main surface microcontroller exchanges commands and data with a paired microcontroller and GSM module with custom firmware (Amtel AT21 and SIM7600 in a Maduino Zero module). The system is programmed to send the last 500 lines (~60 s) of ADV and QMS data and receive commands every 10 minutes. This connection enables real-time visualization of system data for remote troubleshooting and maintenance visit planning (Figure 7).

The lander (Figure 6) consists of an aluminum frame with mounts for the QMS, ADV, and valve control housings, and mounts for the inlets and ADV transducer. The QMS system and control electronics are housed in a 20 cm diameter, 90 cm long schedule 80 PVC tube with power and data connections for the ADV, valve housing, and surface barge. A second microcontroller (Teensy 4.1) controls data acquisition from the ADV and QMS via serial connections, logs data on a microSD card, and communicates with the surface using wired ethernet. A 10 m power and data cable connects the lander to the barge.

Seawater from the high and low inlets is selected for measurement using a servo-controlled 3-way valve. A small PVC diversion valve (McMaster Carr #4757K51) is mated to an underwater servo (Blue Trail SER-2020) using a 3D printed frame and adapter. Actuation and timing is controlled using a microcontroller, which also records pump current draw to assess restrictions in flow due to biofouling. The controller and power system is mounted in a 10 by 30 cm watertight housing. Inlets were positioned 20 and 122 cm above the seabed. The top and bottom inlets were sampled for 7.5 minutes each, alternating continuously through the experiment.

Velocity is sampled at 8 Hz using a Nortek Vector ADV. The adv was mounted at 60 cm above the seabed between the gradient inlets. Signal amplitude and correlation are used to assess data quality.

The QMS system is a Stanford Research Systems RGA-100, configured as a Membrane Inlet Mass Spectrometer (MIMS). The system is based on an underwater quadrupole mass spectrometer design developed in part by Co-PI Wankel [1], [2]. A vacuum chamber containing the QMS is maintained at roughly 1E⁻⁶ Torr using a small turbomolecular pump (Pfeiffer HiPace 30) with a miniature scroll pump (Scroll Labs SVF-2) for rough vacuum. Seawater dissolved gas is introduced to the system via a flat, gas-permeable, Teflon AF2400 membrane mounted on PVDF. Seawater is continuously pushed across the membrane surface using a seabird SBE-5T pump with a flow rate of approximately 3 L min⁻¹. The QMS is set to sample a range of masses with a long dwell time

per mass to increase accuracy and reduce noise, resulting in an acquisition rate of approximately 1 second per mass. Masses measured were 14, 15, 18, 28, 32, 33, 34, 40, and 44, meaning each mass was sampled every 10 seconds.

Description of the Deployment

The system was deployed from June to October 2025. Initial deployment was planned for early June, but was delayed by an intermittent issue with cooling in the surface electronics enclosure, which was solved by a combination of solar reflective paint and addition of a sunshade. The system was deployed at 41.517 N, 70.701 W in a healthy eelgrass bed along the East shore of Uncatena Island in Hadleys Harbor. The harbor opens to the Northeast, facing Woods Hole, a passage with strong ($> 2 \text{ m s}^{-1}$) tidal currents. Prevailing wind direction during the deployment was Southwest. The lander was placed in 2 m depth at mean low water (Figure 8) and the tidal range is roughly 1.5 m. The lander was oriented such that the intakes and ADV transceiver were exposed to the mean current direction and not occluded by the lander systems. The barge was moored 4 m West of the lander (Figure 9) using two anchors in opposition to limit movement due to tide and current, and to maintain Southerly orientation of the solar panels. The site was visited roughly weekly during the deployment for cleaning, sampling, and maintenance.

Co-deployments of calibrated sensors and discrete sampling were used for calibration of the QMS partial pressures for masses with measurable variability and gradient. Two week-long deployments of a Seabird SeapHOx were used to measure Oxygen, and a single two-week deployment of a Pro-Oceanus CO2-Pro was used to measure CO₂. The SeapHOx was deployed on the seabed 2 m upcurrent of the GEMS lander, and the CO2-Pro was deployed below the barge, 4 m from the lander. Discrete samples for methane and hydrogen sulfide concentration were taken once before establishing that concentrations and variability were too small to quantify with the QMS data. Methane samples were taken in gas-tight 60 ml syringes and analyzed using GC-FID on an Agilent-6890 gas chromatograph. Methane concentration at the lower inlet was 20 $\mu\text{mol L}^{-1}$. Hydrogen sulfide samples were taken in gas-tight syringes at the low inlet, fixed as ZnS by addition of zinc acetate and analyzed by the methylene blue technique [3]. Total sulfide concentration was below the limit of detection for this method.

Eelgrass growth samples were taken at the site roughly monthly during the deployment period, continuing a sampling series started at the site in 2021. Eelgrass shoots, epiphytes, and algae were sampled from 3-5 20 cm square quadrats, randomly distributed within 15 m of the GEMS lander. Shoots were counted and measured, then shoots, algae, and epiphytes were dried at 60 C and weighed for biomass assessment.

The deployment was generally successful, but several issues resulted in planned and unplanned maintenance. In the coastal environment, fouling was a constant concern. Growth of algae on the upper and lower inlet screens and on the QMS inlet membrane altered the flow and pressure of water across the inlet, which in turn affected gas transport across the membrane. This was visible in QMS telemetry data as a reduction in partial pressure of gas species; this reduction was used as a diagnostic for site visits to clean the system. The QMS was generally reliable, but the system did shut down unexpectedly 24 h after a lander maintenance due to high QMS filament current triggering an interlock. This was likely due to the release of a small pocket of gas within the system

after the initial evacuation and restart of the system after maintenance. After the event, the system was restarted remotely using the GSM communication system. Another unplanned breakdown was caused by the failure of an undersized DC-DC converter which supplied 12 V power to the valve and ADV modules. High current loads during valve movement caused the converter to fail to a state where 24 V was passed to the ADV and valve, resulting in issues with the valve and ADV. The inlet selector valve had several failures due to repeated actuation causing fatigue in a splined joint in the valve body. The valve was an off-the-shelf commercial 3-way fluid handling unit made from PVC. No test data were available from the manufacturer, but the valve was clearly not designed for continuous use. The valve failed repeatedly after roughly 5000 actuations. Our solution was to treat it as a field-replaceable part for the duration of the deployment, but a more durable valve and a gentle acceleration profile for the servo actuator are necessary to avoid future valve failures.

Data Reduction

Mass spectrometry, velocity, and ancillary data are stored in a single file, rotated every 6 hours. A data reduction package was developed in the R language to validate and parse GEMS file data, normalize and calibrate QMS mass data, use velocity data to model eddy transport, and calculate fluxes using the gradient method.

QMS mass data was normalized to Argon (mass 40) to reduce the effects of flow, pressure, and temperature on gas solubility and QMS signal. A pronounced effect due to inlet biofouling was observed in raw mass signals; this was greatly reduced by normalizing the signals to Argon. Argon normalization also removes physical effects on gas concentration (temperature, air-sea exchange), leaving only biological signals.

Data from co-deployed sensors and concurrent sampling were used for calibration of the QMS signals. A linear model between the Argon-normalized oxygen and CO₂ signals (mass 32:40, mass 44:40, respectively) from the top inlet and the concentration data from the respective sensor (O₂, CO₂) was used to calibrate QMS signals to units of Oxygen and CO₂ concentration.

After calibration, QMS data from each 450 second inlet period were averaged from second 60 to 420 of the period to allow time for flushing water from the previous inlet from the system and stabilization of the QMS signal. Stepwise linear interpolation was used to combine neighboring high and low inlet periods into 15 minute averages for gradient and flux analysis.

ADV velocity data were separated by data type, then velocity data lines were timestamped using count data and corresponding ADV status data lines, checking for malformed and out-of-sequence rows. A rolling Hampel filter was used to flag extreme outlying points, greater than 8 standard deviations from the running median. Gross range filters were then used to remove physically unreasonable values. After preprocessing, noisy or incoherent velocity data was removed by selecting data with greater than 50% correlation. The velocity time series was completed where possible using linear interpolation where gaps were smaller than 1 s, and consecutive 15 minute blocks were flagged for spectral analysis. Data were also divided into separate periods for each new position of the lander after maintenance to allow rotation of axes to minimize mean vertical current. Cross-power spectral density (CPSD) was used to determine covariance of horizontal

and vertical velocity and from that the friction velocity (u^*) term for gradient flux determination. CPSD and u^* were calculated using a vetted procedure in Matlab [4].

Flux was calculated for each 15 minute block using the gradient method [5], [6, W. R. McGillis, C. Langdon, B. Loose, K. K. Yates, and J. Corredor [7]]. Flux is estimated using the chemical gradient ($\frac{dO}{dz'}$) and parameterization of eddy diffusivity (Equation 1). The eddy diffusivity term ($-K_{DO}$) is in turn parameterized using the friction velocity, turbulent length scale, and von Kármán constant (κ , taken as 0.4 here, Equation 2). The turbulent length scale (l) is estimated based on height above the bed surface following McGillis et al. 2011. Continuous estimation of the turbulent length scale was not possible without shear velocity profiles from a co-deployed ADCP. The covariance of the horizontal and vertical current velocity components provided an estimate for the friction velocity (u^*) using the root of the CPSD of horizontal and vertical components ($\overline{u'w'}$, Equation 3).

$$Flux = -K_{DO} \frac{dO}{dz'} \quad (1)$$

$$K_{DO} = u^* \kappa l \quad (2)$$

$$u^* = \sqrt{\overline{u'w'}} \quad (3)$$

Flux was integrated to provide an hourly flux (mmol m⁻² h⁻¹).

Results

QMS Data

Dissolved gas measurements over time from the GEMS system (Figure 10) show clear variability in dissolved oxygen and carbon dioxide concentrations and gradients. Low concentration and interference with ions from other species make determination of methane, nitrogen, and hydrogen sulfide fluxes difficult or impossible. Discrete measurements of methane showed low but measurable concentrations at the site (20 µmol L⁻¹), but interference with peaks from water and oxygen (mass 16) made reliable determination impossible. Discrete measurements of hydrogen sulfide showed no measurable H₂S at the site, so we believe any signal at mass 34 is likely a known interference with oxygen. We were able to greatly reduce the signal to noise ration in QMS data for the 2025 deployment as compared to the 2022 deployment (Figure 11) by improving the microcontroller-based data acquisition system, adjusting the QMS chamber pressure, and reducing electrical noise. We found that normalizing signals to Argon (mass 40) greatly improved signal stability. Argon is similar in physical behavior to the other gasses of interest, but is not modified by ecosystem processes. Normalizing to argon removes much of the effect of environmental factors like temperature, pressure, and air-sea gas exchange, and system factors like flow rate, membrane permeability and biofouling (Figure 12).

Calibration

Time-correlated data from co-deployed sensors was used for calibration. A linear fit between the argon-normalized mass of interest and calibrated sensor data was used to generate a calibration curve (Figure 15). This produced a reasonable fit between the calibrated GEMS and sensor data

(Figure 16). Cross-calibration with co-deployed sensors balances attempting to sample the same water concurrently with GEMS and disturbing eddy propagation and flow around and within the GEMS system. We chose to co-deploy sensors 2 m in the mean upcurrent direction to avoid disturbing eddy propagation. If the co-deployed sensors could sample the GEMS inlets directly without disturbing current or sample loop flow, the calibration uncertainty may be reduced.

Gradients and Fluxes

Hourly fluxes for the duration of the deployment were determined for Oxygen (Figure 17) and Carbon Dioxide. Fluxes show a clear diel cycle (Figure 18). Averaging these gradients by hour of solar day (Figure 19) shows a mean daily maximum oxygen gradient of $\pm 10 \text{ mmol m}^{-4}$. A clear diel cycle is apparent in the oxygen (Figure 20) and carbon dioxide (Figure 21) fluxes. Monthly patterns in the diel oxygen fluxes (Figure 23) show larger daily variability during summer months, when more light is available and water temperature is higher. The relationship between oxygen and carbon dioxide fluxes is complex (Figure 22). Speciation of CO_2 in the carbonate system and the balance of system respiration and photorespiration likely drive this relationship. Neither pH nor alkalinity were measured concurrently with dissolved gasses, so it is difficult to quantify inorganic carbon among carbonate species (CO_2 , CO_3^{2-} , HCO_3^-). Monthly and daily (Figure 24) estimates of net ecosystem metabolism show that while net fluxes vary on multiple timescales, the net metabolism of the system is close to zero.

Eelgrass Growth Data

Eelgrass growth measured as areal density and length of annual shoots was measured at the Hadleys Harbor site semi-monthly for the duration of the project. Growth data are presented in Figure 25. Growth trends are generally consistent from year to year. Maximum shoot biomass density and blade length occur late in the summer growth season.

Figures

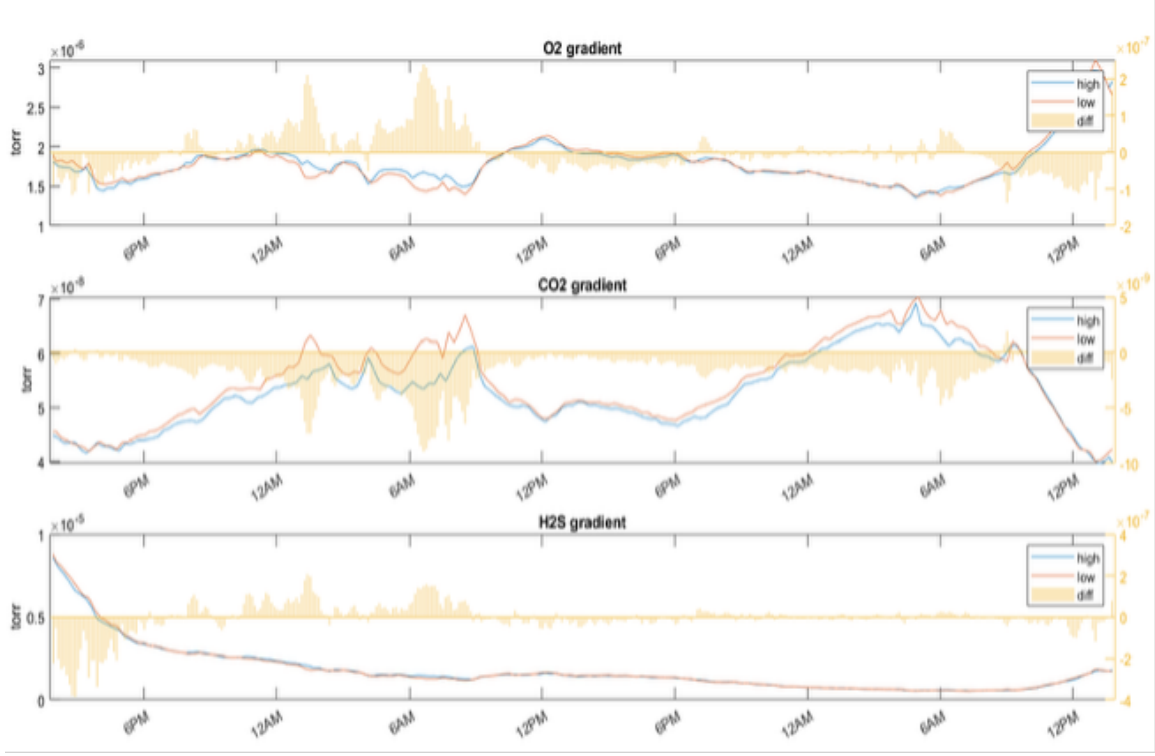


Figure 1: The initial gradients measured by the prototype GEMS system during the 2021 deployment. Blue traces are the upper (1.1 m) height, red are the lower (0.2 m) height (left axis), and the yellow bars indicate the magnitude of the gradient through time (right axis). Notice the opposite magnitudes of the carbon dioxide (CO_2 , middle) and oxygen (O_2 , top) gradients consistent with diel rates of photosynthesis and respiration. The hydrogen sulfide (H_2S , bottom) gradients appear to co-vary with the oxygen gradients. We now believe this indicates mass interference with oxygen in the QMS.



Figure 2: The GEMS power, data and telemetry platform with undergraduate Guest Student Natalia Wierzbicki and Summer Student Fellow (NSF REU) Ryan Galusha. Natalia and Ryan helped build the platform for the 2022 deployment. For 2025, the platform was outfitted with improved power and data systems, including more reliable communication with the lander, a new GSM/GPS module transmitting more telemetry data, and a safety switch for the wind turbine.

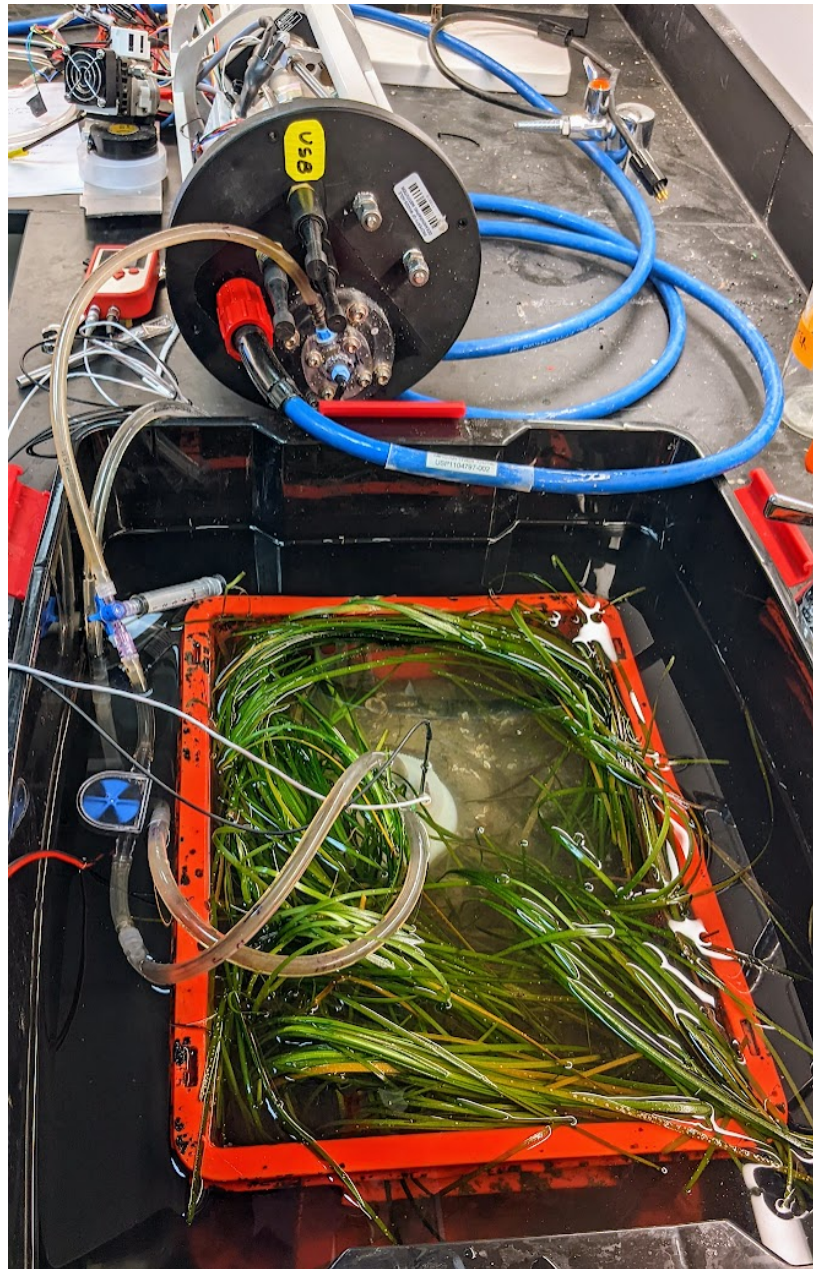


Figure 3: The GEMS set up for measurement of denitrification in *Zostera marina* (eelgrass) mesocosms. The evolution of ^{15}N -labeled nitrate to labeled nitrogen gas was measured using the GEMS spectrometer in small, open bottom chambers. Argon was added to track loss of the label and nitrogen from the chamber system.

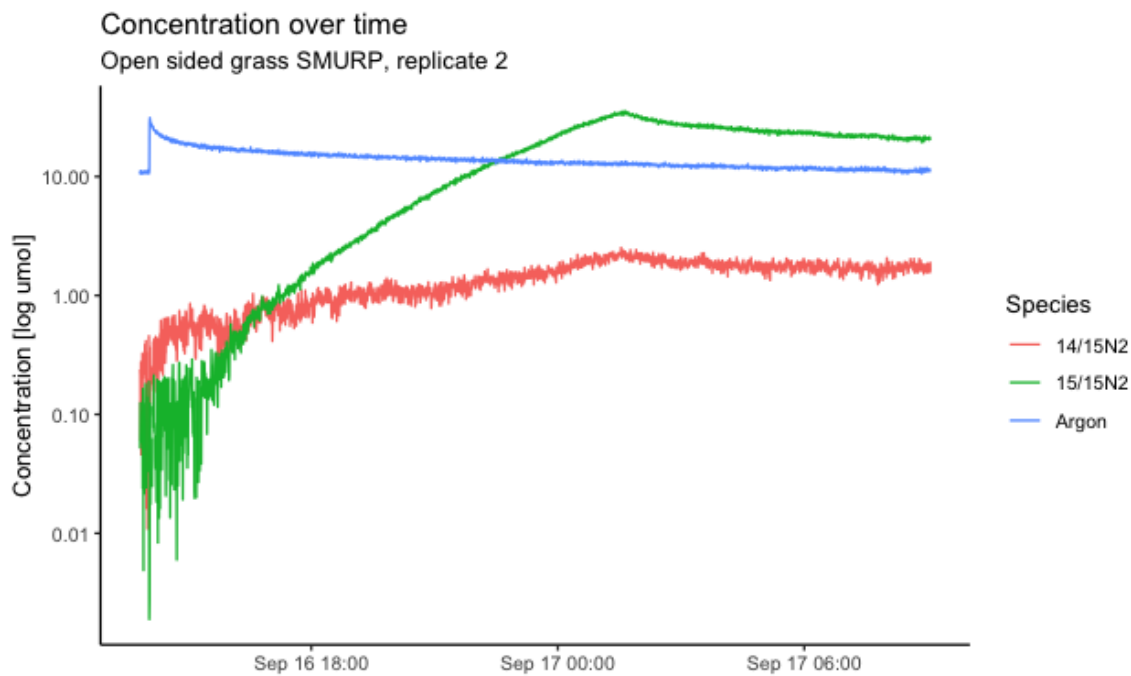


Figure 4: Evolution through time of single- and doubly-labeled nitrogen and argon tracers during a denitrification experiment in an eelgrass mesocosm.

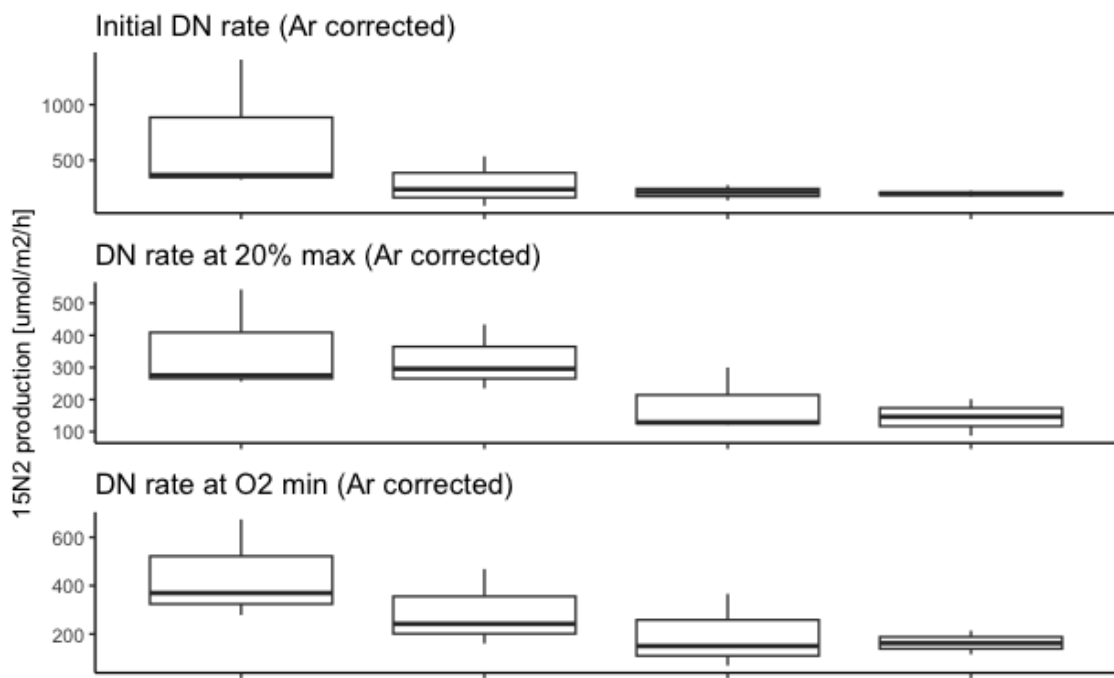


Figure 5: Denitrification rates for three replicates of 4 experimental treatments at different time points during the experiments. Open crates have 4 cm open mesh sides and bottom and are lined with coir to prevent sediment loss. Closed crates have solid sides and bottom. Grass crates have healthy seagrass. Sediment crates have identical substrates with no seagrass. Rates from top to bottom are determined 2.5 hours after label injection, at 0.2 of the time of maximum $^{15}\text{N}_2$ concentration, and at the time anoxia is reached.

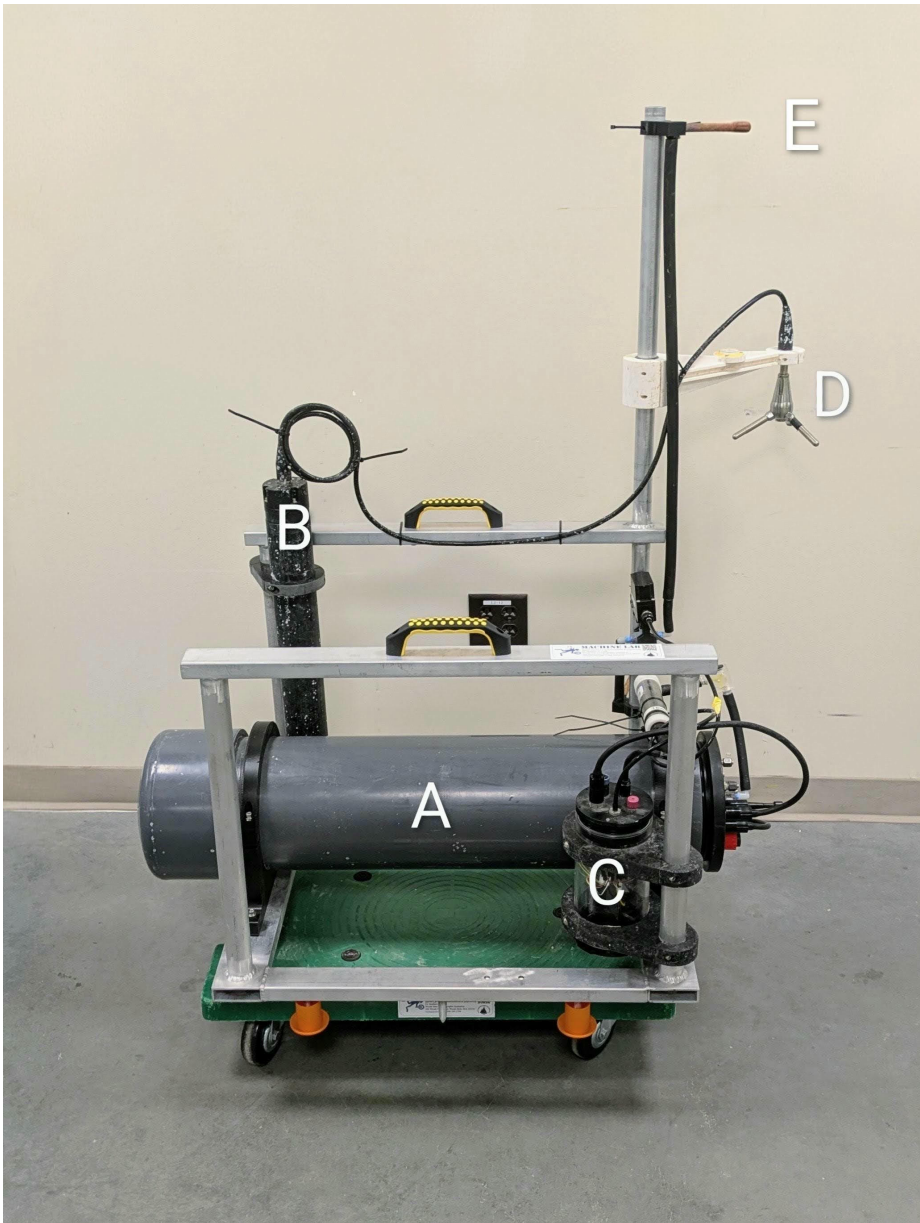
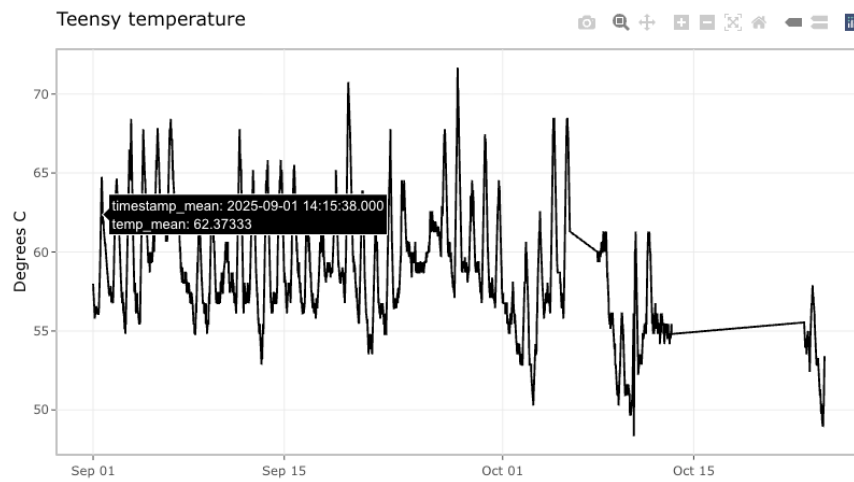


Figure 6: The GEMS lander, redesigned for the 2025 deployment. The central housing (A) contains the QMS, power handling and system microcontroller. The ADV transducer (D) and housing (B) collect velocity data at mid-height. The valve housing (C) contains control and power electronics for the system pump and servo controlled valve for switching between high (E) and low inlets.

Teensy Temp

Junction temp of Surface teensy. Runs at 50C at room temp. >95C kills teensies.



On this page

- [Get Data](#)
- [Status](#)
- [GEMS Status changes](#)
- [Post times](#)
- [Teensy Temp](#)
- [Seawater temp](#)
- [Battery](#)
- [Turbo](#)
- [RGA](#)
- [ADV](#)
- [IMU data](#)
- [Data issues](#)

Seawater temp

Using ADV sensor at mid-height

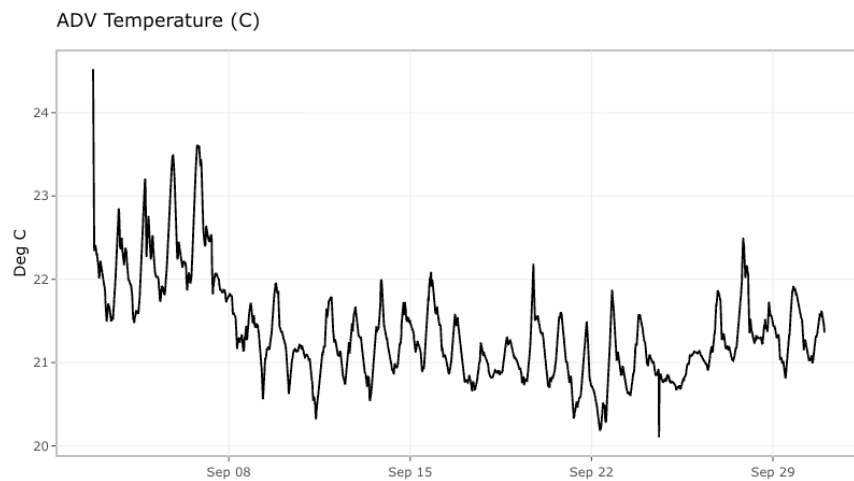


Figure 7: For the 2025 deployment, we created a publicly accessible website summarizing all telemetry data (https://blongworth.github.io/GEMS_status/). The site was mostly used to monitor the system and troubleshoot issues. The site uses a simple API to collect data from a WHOI-hosted server, which in turn communicates directly with GEMS and stores telemetry data.



Figure 8: The GEMS power, data and telemetry platform (top left) and GEMS lander (bottom right). A 10m cable providing 24V power and ethernet-based data runs between the platform and lander.



Figure 9: The GEMS platform during the 2025 deployment. Samuel Koeck (MIT/WHOI PhD student) is above the lander deployment location.

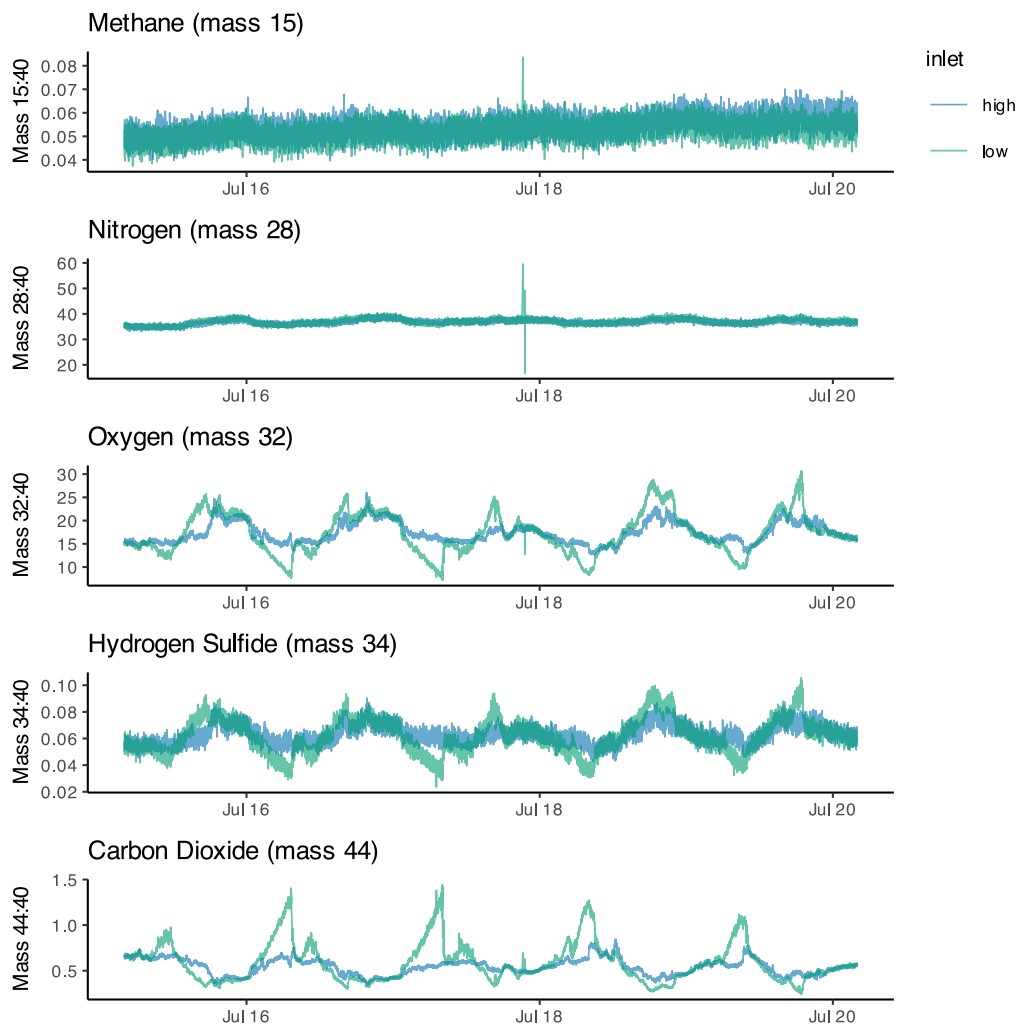


Figure 10: RGA signals for masses of interest. Each mass is measured approximately every 10 s. Mass traces are colored by the selected inlet; blue indicates the upper or “high” inlet, and green indicates the bottom or “low” inlet. A five day period of the deployment was chosen to highlight diel cycles. Each signal is normalized to mass 40 (Argon) to control for effects of temperature, pressure, and biofouling. The mass 34 signal is likely an interference with Oxygen, rather than a true hydrogen sulfide signal.

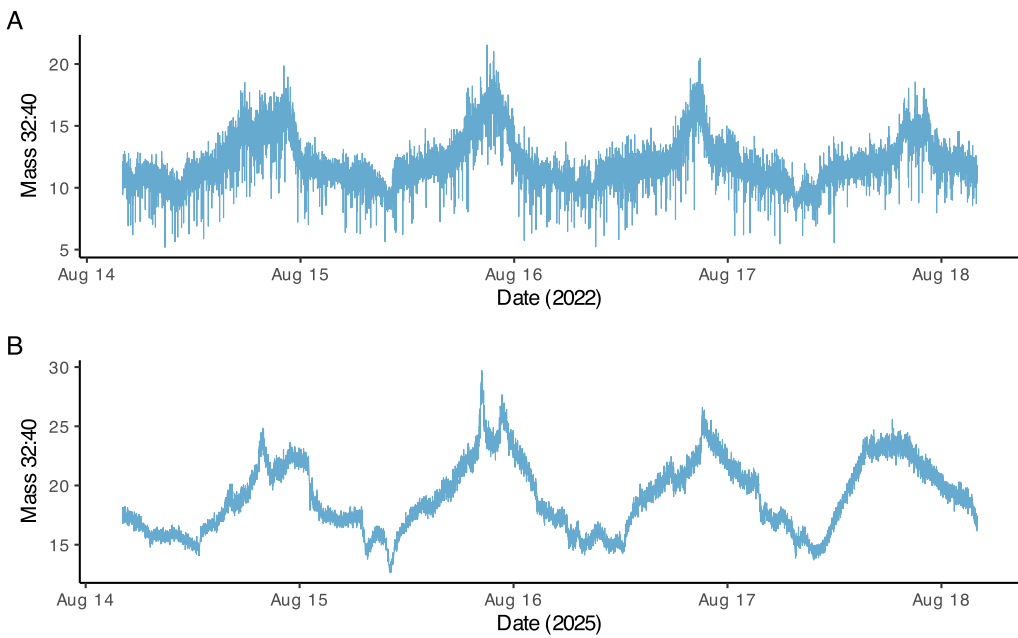


Figure 11: Comparison of QMS signal noise for argon-normalized oxygen at the high inlet between 2022 (A) and 2025 (B) deployments. Signal noise was greatly reduced for the 2025 deployment, improving the accuracy and limit of detection for gradient determination.

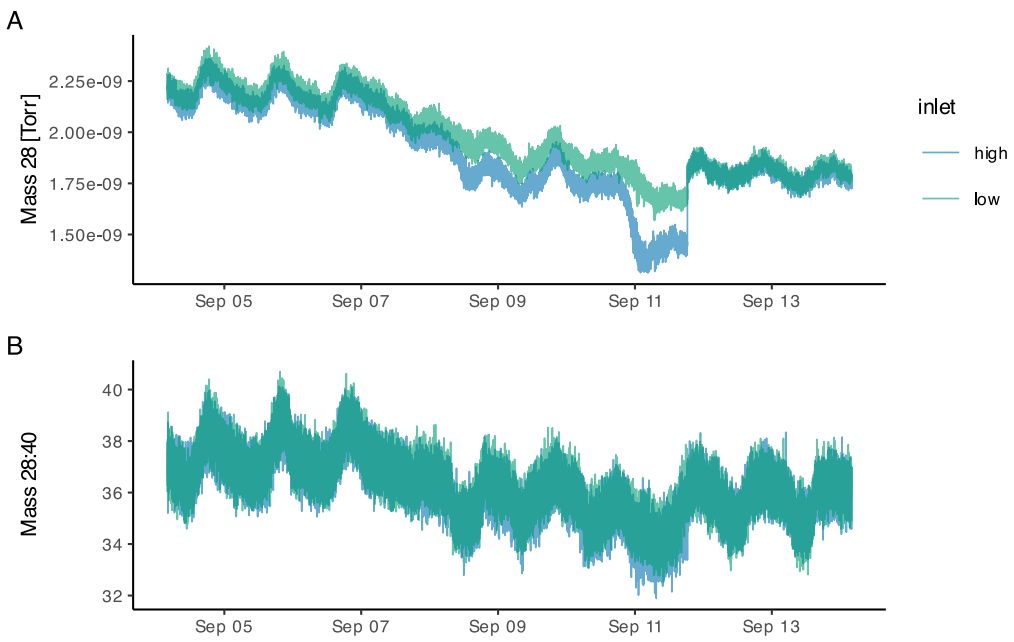


Figure 12: This figure shows Nitrogen (mass 28) un-normalized (A) and normalized (B) using concurrent Argon (mass 40) measurements across a period of increasing biofouling at the high inlet (blue), followed by cleaning the inlets on Sept. 11. Normalizing measured masses to Argon controls for physical effects on gas solubility and membrane transport. Gas transport across the membrane is affected by temperature, pressure and water flow rate.

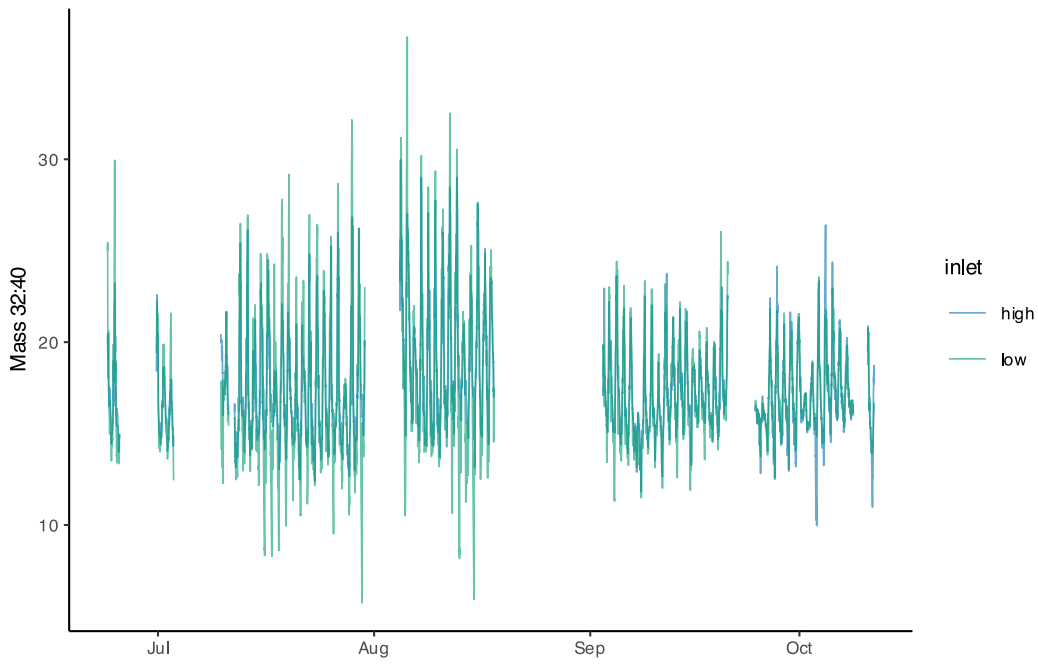


Figure 13: A record of the argon-normalized oxygen signal at the high (blue) and low (green) inlets for the duration of the deployment. Maintenance periods and times when the data were known to be poor due to system issues have been removed.

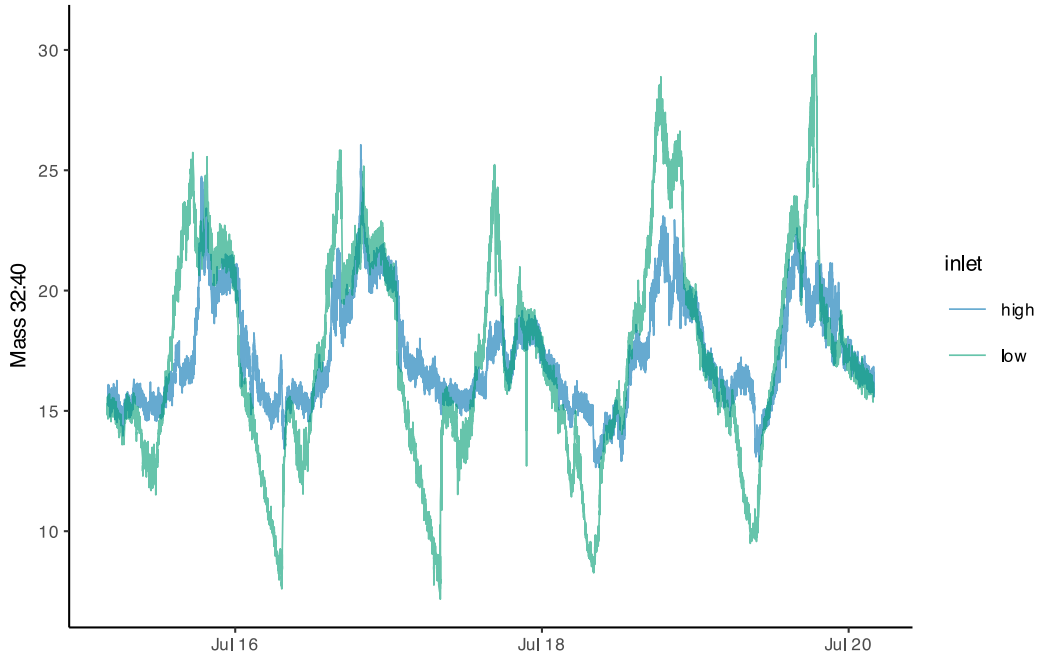


Figure 14: The argon-normalized oxygen signal for July 16-20, showing a clear gradient between the high (blue) and low (green) inlets. The diel variability of oxygen at the low inlet is higher due to proximity to the eelgrass and seabed.

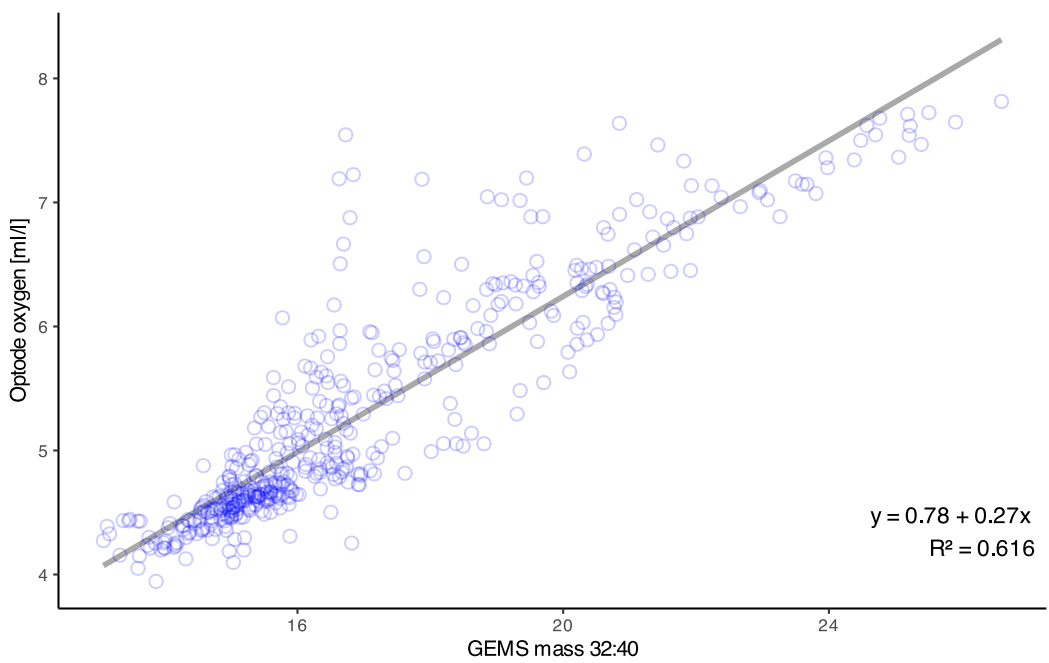


Figure 15: Oxygen calibration data for the SeapHOx codeployment. SeapHOx optode data is compared to GEMS mass 32:40 at the high inlet, which is nearer in height to the SeapHOx inlet (80cm). The line shows linear model fit.

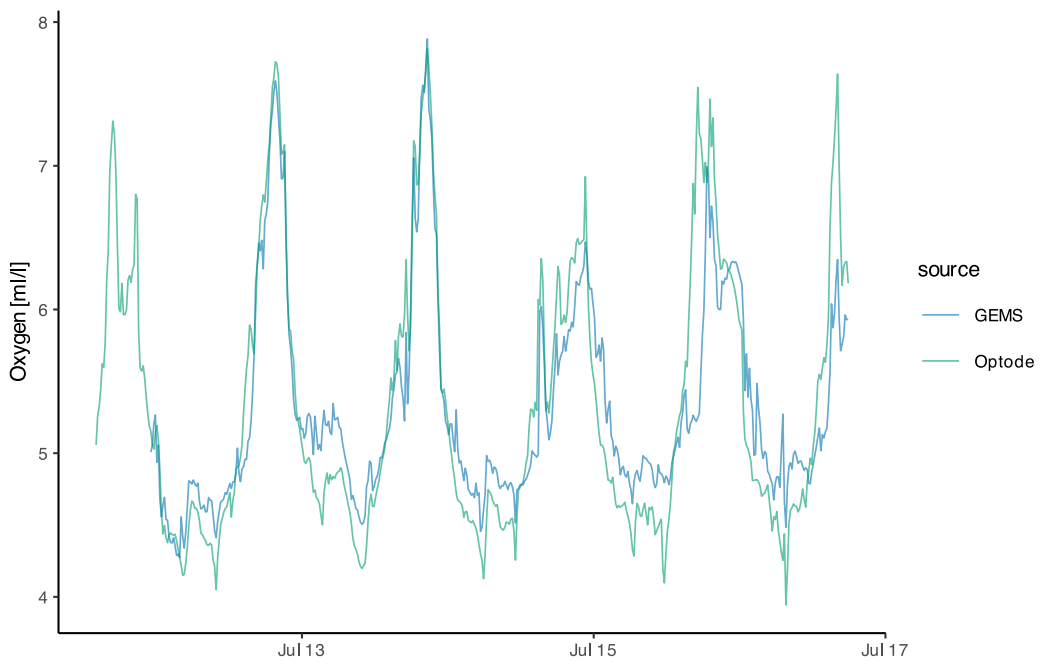


Figure 16: SeapHOx optode (green) and fitted GEMS oxygen at the high inlet (blue) over the codeployment time period. Fitted RGA Oxygen data shows a reasonable match to the SeapHOx optode data for the codeployment period. The peak attenuation in the GEMS signal is likely due to the intermittent signal from inlet switching.

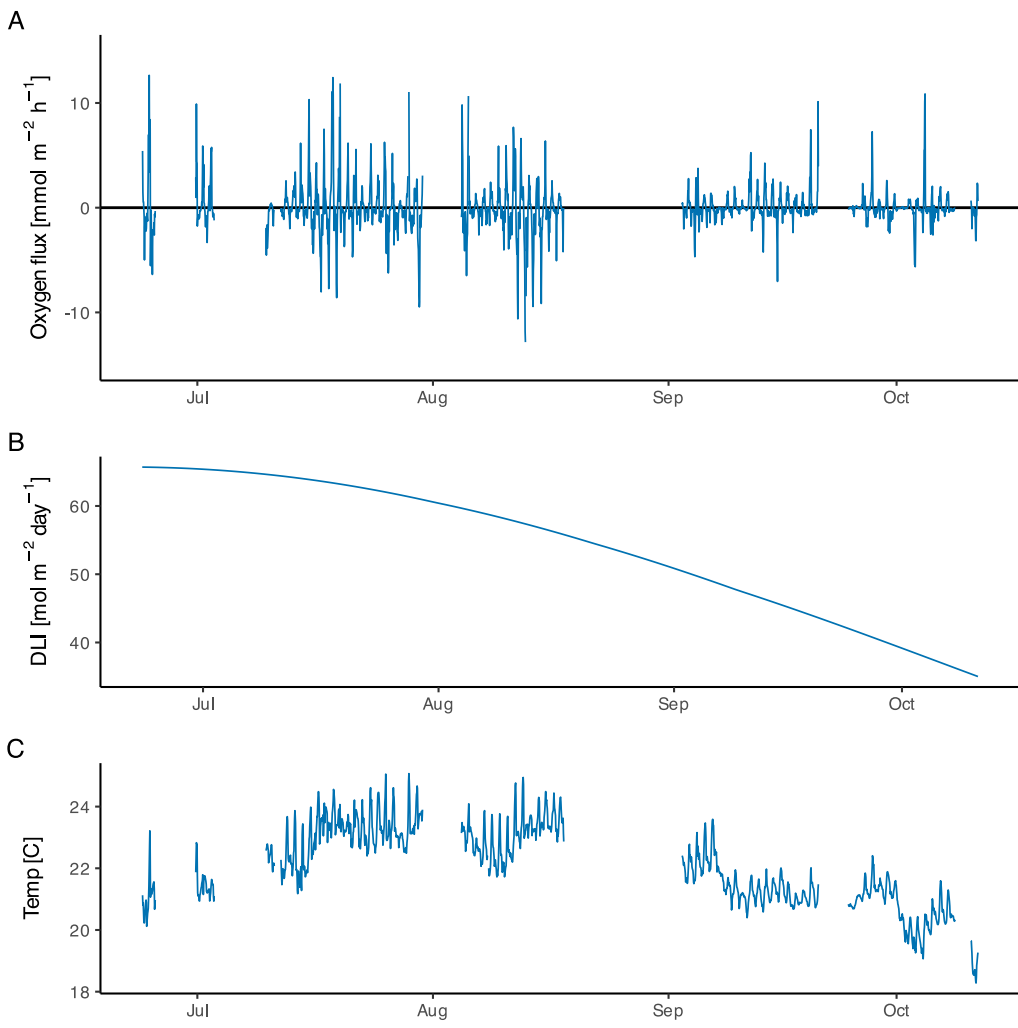


Figure 17: Hourly oxygen flux (A) for the duration of the deployment. Maintenance periods and times when the data were known to be poor due to system issues have been removed. estimated daily light integral (DLI, B) and seawater temperature at mid height (C) for comparison. Flux decreases with decreasing light and temperature. No light sensor was codeployed with GEMS, therefore photosynthetically active radiation (PAR) and DLI are estimated from modeled, cloud-free insolation. A high flux outlier on July 19 believed to be caused by fouling was removed from the plot.

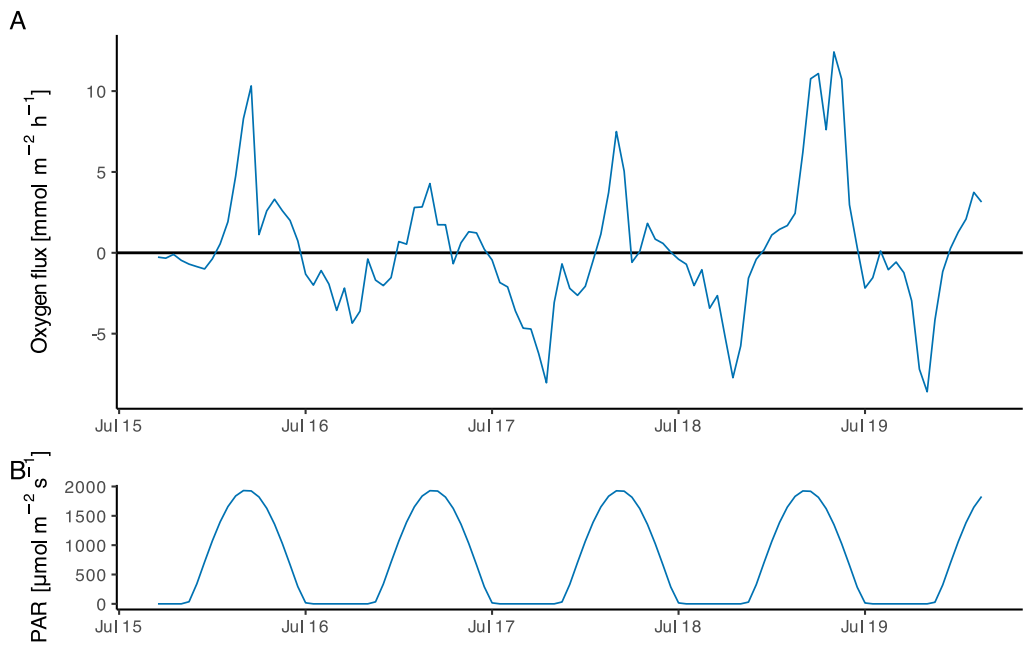


Figure 18: Oxygen flux (A) with predicted PAR (B) for comparison for the period July 15-20. Upward flux aligns with peak daily light. Respiration flux increases through the dark hours. Fluxes have strong daily variability.

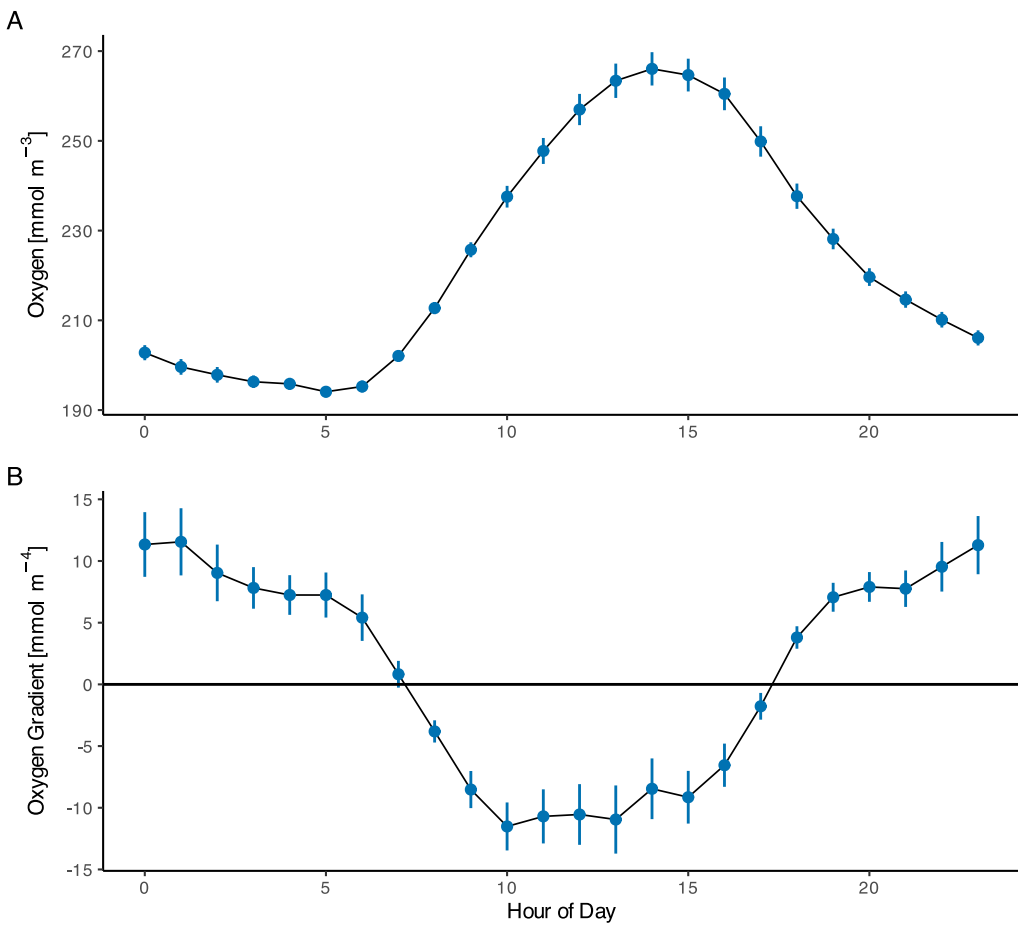


Figure 19: GEMS oxygen concentration (A) and gradient (B) aggregated across the deployment by hour of day. Hour is adjusted to the mean solar noon for the deployment. Oxygen concentration is the mean across both inlets. Gradient is estimated using the difference between high and low inlets over the difference in inlet height.

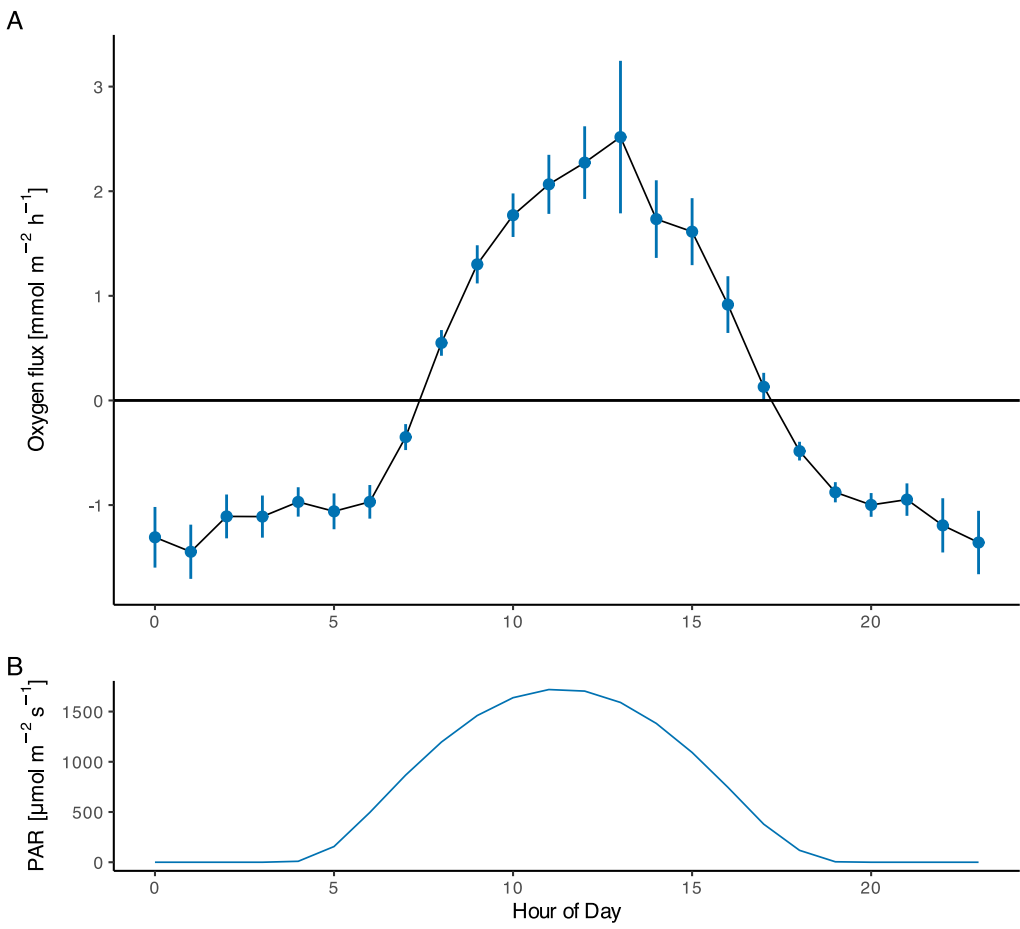


Figure 20: GEMS oxygen flux (A) and predicted PAR (B) aggregated hourly for the duration of the deployment. Hour is adjusted to the mean solar noon for the deployment.

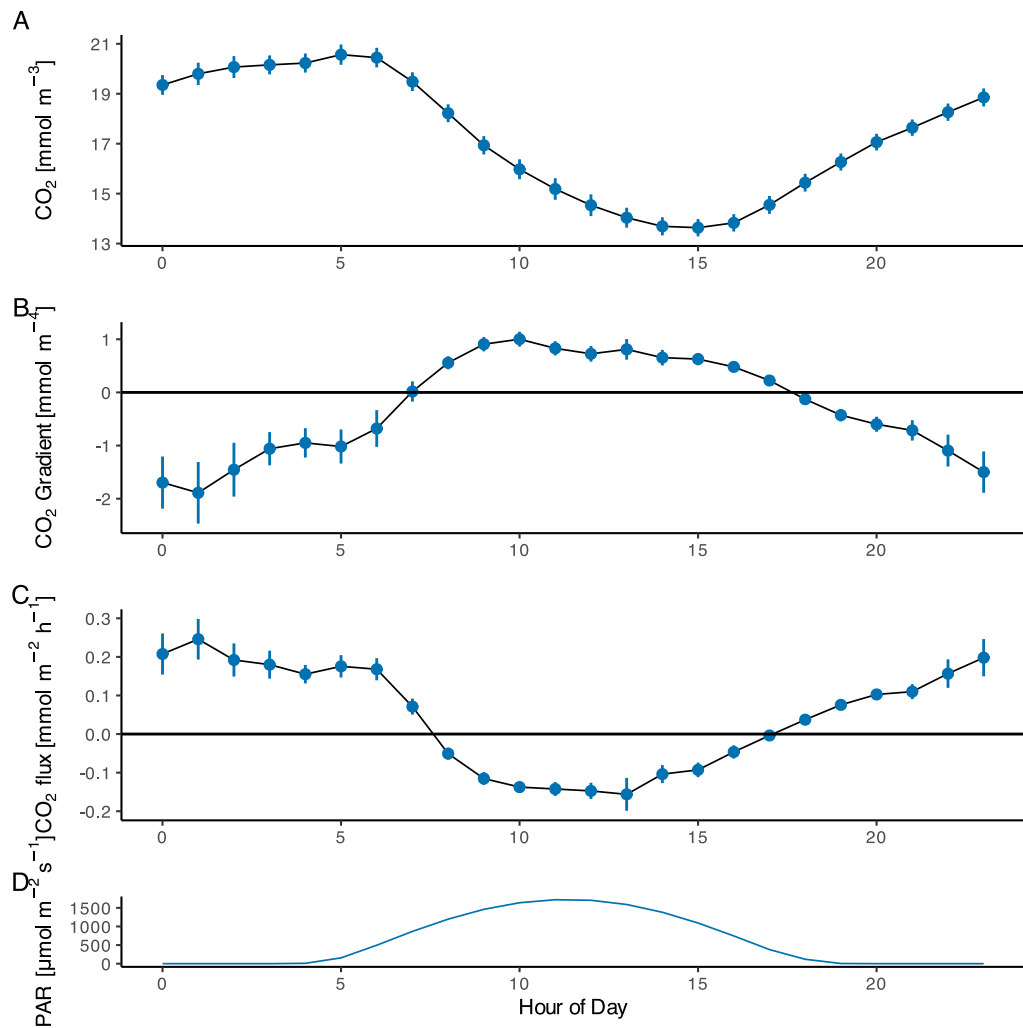


Figure 21: GEMS carbon dioxide concentration (A) and gradient (B) and flux (C) aggregated across the deployment by hour of day. Hour is adjusted to the mean solar noon for the deployment, and predicted PAR is shown in (D). CO₂ concentration is the mean across both inlets. Gradient is estimated using the difference between high and low inlets over the difference in inlet height.

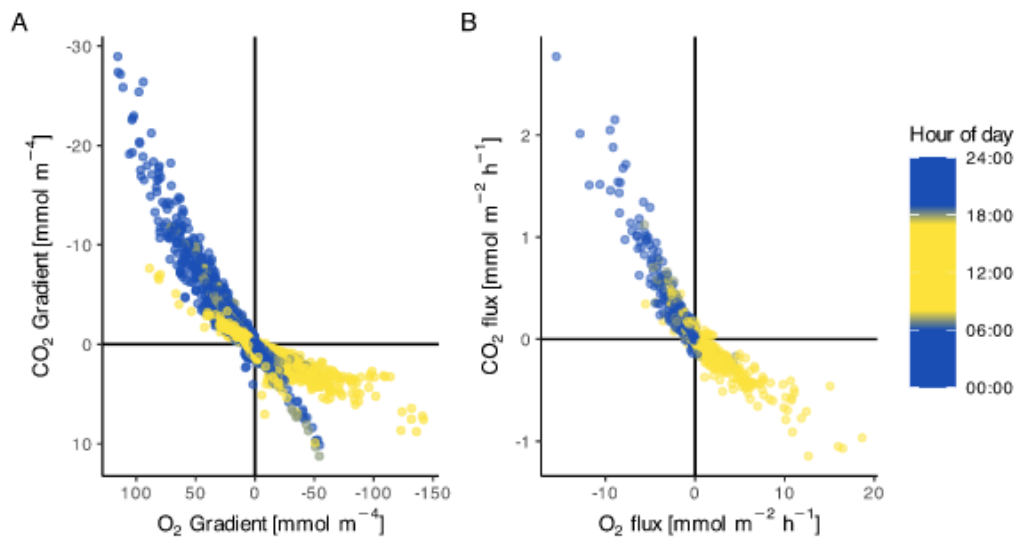


Figure 22: The relationship between CO₂ and O₂ vertical gradients (A) and flux (B), colored by predicted PAR. Gradient scales are reversed to place in the same frame of reference as flux.

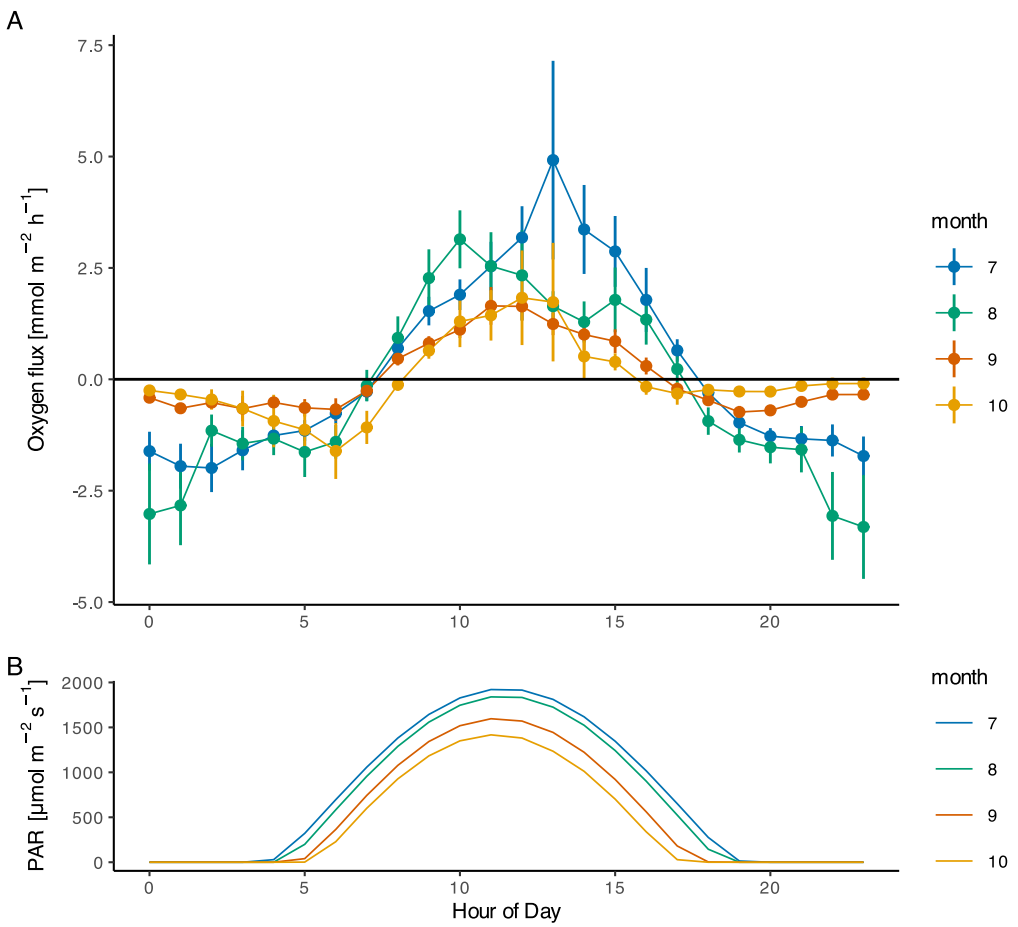


Figure 23: GEMS oxygen flux (A) and predicted PAR (B) aggregated hourly and separated by month. Hour is adjusted to the mean solar noon for the deployment. June data is not shown due to bias from only 3 days of data acquisition.

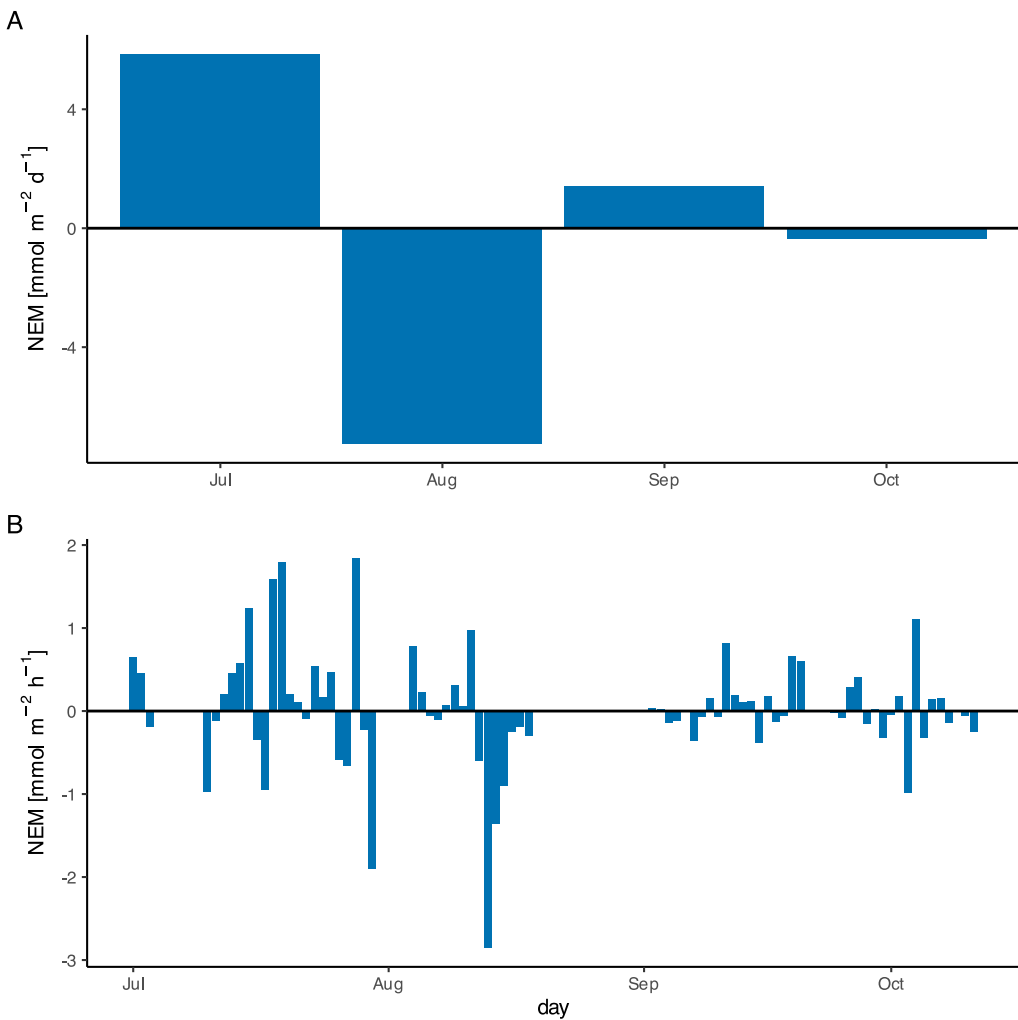


Figure 24: Oxygen flux integrated by day (A) and by month (B) for the deployment period to provide an estimate of net ecosystem metabolism (NEM). The benthic system at Naushon Island shows variability on daily and monthly scales, but the system is close to net neutral over time.

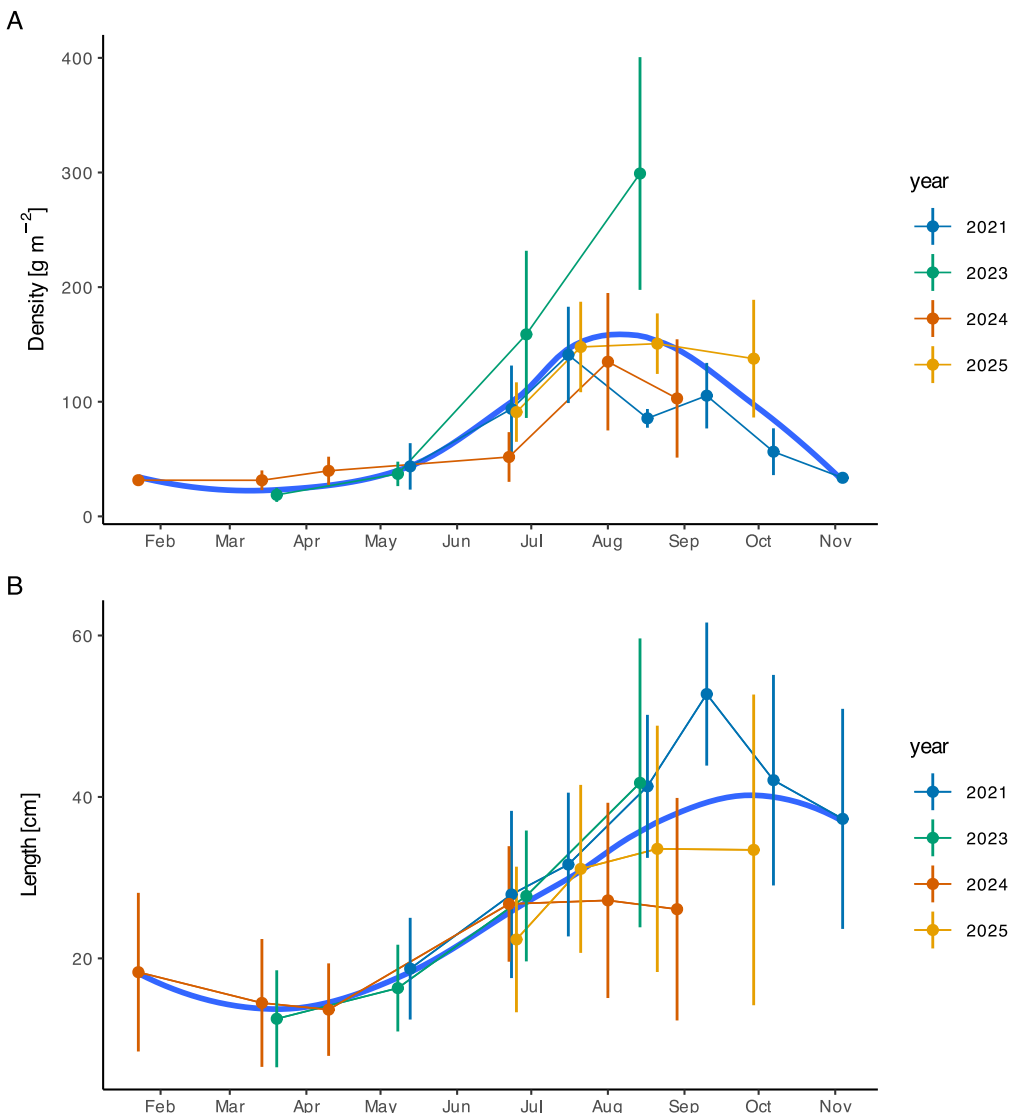


Figure 25: Naushon eelgrass shoot biomass (A) and shoot length (B) data by year. Eelgrass was sampled from 3-5 20 cm² quadrats. Point error bars are the standard deviation of quadrats for mass and count and the standard deviation of all blade lengths for length. The fit line is a loess fit through all data.

Bibliography

- [1] S. D. Wankel *et al.*, “New constraints on methane fluxes and rates of anaerobic methane oxidation in a Gulf of Mexico brine pool via in situ mass spectrometry,” *Deep Sea Research Part II: Topical Studies in Oceanography*, vol. 57, no. 21, pp. 2022–2029, Nov. 2010, doi: 10.1016/j.dsr2.2010.05.009.

- [2] S. D. Wankel *et al.*, “Influence of subsurface biosphere on geochemical fluxes from diffuse hydrothermal fluids,” *Nature Geoscience*, vol. 4, no. 7, pp. 461–468, Jul. 2011, doi: 10.1038/ngeo1183.
- [3] J. D. Cline, “SPECTROPHOTOMETRIC DETERMINATION OF HYDROGEN SULFIDE IN NATURAL WATERS1,” *Limnology and Oceanography*, vol. 14, no. 3, pp. 454–458, May 1969, doi: 10.4319/lo.1969.14.3.0454.
- [4] M. H. Long, “Aquatic Biogeochemical Eddy Covariance Fluxes in the Presence of Waves,” *Journal of Geophysical Research: Oceans*, vol. 126, no. 2, p. e2020JC016637, Feb. 2021, doi: 10.1029/2020JC016637.
- [5] J. Coogan, J. E. Rheuban, and M. H. Long, “Evaluating benthic flux measurements from a gradient flux system,” *Limnology and Oceanography: Methods*, vol. 20, no. 4, pp. 222–232, Apr. 2022, doi: 10.1002/lom3.10482.
- [6] Y. Takeshita *et al.*, “Assessment of net community production and calcification of a coral reef using a boundary layer approach,” *Journal of Geophysical Research: Oceans*, vol. 121, no. 8, pp. 5655–5671, Aug. 2016, doi: 10.1002/2016JC011886.
- [7] W. R. McGillis, C. Langdon, B. Loose, K. K. Yates, and J. Corredor, “Productivity of a coral reef using boundary layer and enclosure methods: CORAL REEF PRODUCTIVITY,” *Geophysical Research Letters*, vol. 38, no. 3, p. n/a–n/a, Feb. 2011, doi: 10.1029/2010GL046179.